REPORT DOCUMENTATION PAGE

Form Approved
OMB No. 0704-0188

1. REPORT DATE *(DD-MM-YYYY)*	2. REPORT TYPE	3. DATES COVERED *(From - To)*
05-02-2007	REPRINT	

4. TITLE AND SUBTITLE
Passive Optical Diagnostic of Xe-propelled Hall Thrusters. I. Emission Cross Section

5a. CONTRACT NUMBER

5b. GRANT NUMBER

5c. PROGRAM ELEMENT NUMBER
61102F

6. AUTHOR(S)
Y. Chiu, B. L. Austin, S. Williams, R. A. Dressler, and G. F. Karabadzhak*

5d. PROJECT NUMBER
2303

5e. TASK NUMBER
RS

5f. WORK UNIT NUMBER
A1

7. PERFORMING ORGANIZATION NAME(S) AND ADDRESS(ES)
Air Force Research Laboratory/VSBXT
29 Randolph Road
Hanscom AFB MA 01731-3010

8. PERFORMING ORGANIZATION REPORT NUMBER
AFRL-VS-HA-TR-2007-1007

9. SPONSORING / MONITORING AGENCY NAME(S) AND ADDRESS(ES)

10. SPONSOR/MONITOR'S ACRONYM(S)

11. SPONSOR/MONITOR'S REPORT NUMBER(S)

12. DISTRIBUTION / AVAILABILITY STATEMENT
Approved for Public Release; Distribution Unlimited

*TSNIIMASH, Pionerskaya, Korolev, Moscow Region, Russia

13. SUPPLEMENTARY NOTES
REPRINTED FROM: Journal of Applied Physics, Vol 99, 113304 (2006).

14. ABSTRACT

This paper presents a set of xenon apparent emission excitation cross sections for emission lines that have diagnostic value in the analysis of Xe-propelled Hall thruster plasmas. Emission cross sections are presented for three excitation processes involving ground-state xenon atoms: e^-+Xe, Xe^+ +Xe, and Xe^{2+}+Xe. The cross sections are derived from luminescence spectra produced at single-collision conditions. Apparent emission excitation cross sections are tabulated for 12 visible and 8 near-infrared lines for electron energies ranging from 10 to 70 eV. In case of the near-infrared lines, radiation trapping effects are accounted for by measuring the detailed pressure dependence of the apparent emission cross sections and extrapolating to zero pressure. A semiempirical expression for the pressure dependence is derived that allows zero-pressure extrapolation from threshold to 70 eV. Ion-induced cross sections are reported for the same emission lines at an energy per unit charge E/q of 300 eV, chosen for typical Hall thruster operating voltages. Radiation trapping effects are negligible for the ion emission excitation cross sections between 0.1 and 2.0 mTorr in the present luminescence experiment. © *2006 American Institute of Physics.*

15. SUBJECT TERMS
Electron emission excitation cross sections, Ion collision-induced emission excitation cross sections, Xe, Electric Propulsion, Optical plasma diagnostic, Hall thrusters, Xenon plasma

16. SECURITY CLASSIFICATION OF:			17. LIMITATION OF ABSTRACT	18. NUMBER OF PAGES	19a. NAME OF RESPONSIBLE PERSON
a. REPORT	b. ABSTRACT	c. THIS PAGE			R. Dressler
UNCLAS	UNCLAS	UNCLAS	SAR		19b. TELEPHONE NUMBER *(include area code)* 781-377-2332

JOURNAL OF APPLIED PHYSICS 99, 113304 (2006)

Passive optical diagnostic of Xe-propelled Hall thrusters. I. Emission cross sections

Yu-hui Chiu, Brad L. Austin,[a] Skip Williams,[b] and Rainer A. Dressler
Air Force Research Laboratory, Space Vehicles Directorate, Hanscom AFB, Massachusetts 01731

George F. Karabadzhak
TSNIIMASH, Pionerskaya 4, Korolev, Moscow region, 141070, Russia

(Received 23 August 2005; accepted 13 March 2006; published online 9 June 2006)

This paper presents a set of xenon apparent emission excitation cross sections for emission lines that have diagnostic value in the analysis of Xe-propelled Hall thruster plasmas. Emission cross sections are presented for three excitation processes involving ground-state xenon atoms: e^-+Xe, $Xe^+ + Xe$, and $Xe^{2+}+Xe$. The cross sections are derived from luminescence spectra produced at single-collision conditions. Apparent emission excitation cross sections are tabulated for 12 visible and 8 near-infrared lines for electron energies ranging from 10 to 70 eV. In case of the near-infrared lines, radiation trapping effects are accounted for by measuring the detailed pressure dependence of the apparent emission cross sections and extrapolating to zero pressure. A semiempirical expression for the pressure dependence is derived that allows zero-pressure extrapolation from threshold to 70 eV. Ion-induced cross sections are reported for the same emission lines at an energy per unit charge E/q of 300 eV, chosen for typical Hall thruster operating voltages. Radiation trapping effects are negligible for the ion emission excitation cross sections between 0.1 and 2.0 mTorr in the present luminescence experiment. © *2006 American Institute of Physics.*
[DOI: 10.1063/1.2195018]

I. INTRODUCTION

Hall effect thrusters (HETs) are high-specific impulse alternatives to chemical propulsion systems of spacecraft. In HETs, a gas, typically xenon or krypton, is efficiently ionized in a discharge, and positive ions are electrostatically accelerated to generate thrust. The performance, plasma characteristics, and durability of HETs are extensively evaluated both in ground-based test facilities and in space. Basic characteristics of HET plasmas such as charge species densities and temperatures have been traditionally measured by various plasma probes. However, at HET conditions, traditional plasma-probe diagnostics are affected by problems such as the perturbation of the local environment by the probe, the complexity associated with interpreting the probe characteristics, and detrimental effects in regions of high temperatures (e.g., in the HET discharge). Consequently, HET plasma parameters reported from probe experiments exhibit significant disparities. Optical plasma diagnostics circumvent these problems and are thus an attractive alternative to probe measurements.

It has already been demonstrated that optical emission spectra observed in the HET discharge and plume can provide important information on the thruster plasma operating conditions, thereby permitting predictions of the thruster microparameters based on short duration, nonintrusive experiments. Passive optical experiments on HETs have been used to investigate general emissive properties[1–4] of HET plasmas, plasma properties in oscillatory[5–8] and transient[9] operating modes, and thruster body erosion characteristics.[10–12] Attempts have been made to determine the effective electron temperature,[13,14] the electron energy distribution,[15] and the atomic xenon number density and excitation rates for xenon species[16] using passive optical approaches. In all these cases, a plasma collisional radiation model (CRM) was required to quantify parameters from the radiation measurements. A key component of such a model is a set of emission cross sections associated with the energy transfer processes that lead to population of states that radiatively relax through emission in the spectral region of interest. Proper implementation of a CRM has been primarily hampered by the lack of a comprehensive cross section set.

The present paper focuses on emission excitation cross sections for Xe-propelled HETs. Optical radiation in a Xe HET plasma arises from electron and ion-atom collisions, of which the most important contributors can be assumed to be

$$e^- + Xe \rightarrow Xe^* + e^- \tag{1}$$

$$\rightarrow Xe^{q+*} + (q+1)e^-, \tag{2}$$

$$e^- + Xe^+ \rightarrow Xe^{q+*} + qe^-, \tag{3}$$

$$e^- + Xe^m \rightarrow Xe^* + e^- \tag{4}$$

$$\rightarrow Xe^{q+*} + (q+1)e^-, \tag{5}$$

$$Xe^+ + Xe \rightarrow Xe^{+*} + Xe^*, \tag{6}$$

[a]Present address: AFSC/SESD, 9700 G Avenue SE, Kirtland AFB, NM 87117.
[b]Present address: AFRL/PRAS, 1950 Fifth Street, Wright Patterson AFB, OH 45433.

$$Xe^{2+} + Xe \rightarrow Xe^{2+*} + Xe^{*} \quad (7)$$

$$\rightarrow Xe^{+*} + Xe^{+*}. \quad (8)$$

The asterisks in processes (1)–(8) signify excited species that either lead to optical emissions or long-lived metastables that transfer the excitation in subsequent electronic or atomic collisions. q defines the charge state of the respective ion. Superscript m indicates metastable states. Due to the size and relativistic nature of the xenon atom, accurate theoretical computations of excitation cross sections are highly challenging. Approximate models, including the distorted wave approximation and a classical approach by Gryzinski[17] and Bauer and Bartky,[18] have been demonstrated to lead to a broad range of predictions. Colonna *et al.*[19] modeled excitation cross sections for Xe $5p^5 6s$ levels from the ground state using such methods, which resulted in differences ranging from a factor of 2 for optically allowed transitions to factors of 3–4 for forbidden transitions. For transitions between excited states, the uncertainty can be expected to be even higher. A clear validation of a CRM based on such estimated cross sections thus has proven to be very difficult.

While theoretical approaches normally determine direct excitation or level-transition cross sections, optical experiments generally produce apparent emission cross sections that include excitation via all possible cascades from upper states. (Nonoptical approaches, such as electron and ion energy loss experiments, do not have the resolution required to resolve the individual xenon states.) The use of experimental apparent cross sections in a CRM reduces considerably the complexity of a model that predicts optical spectra because the complex web of level-to-level kinetics does not have to be treated explicitly since a large fraction of it is inherently incorporated in the apparent emission cross sections. Fons and Lin[20] measured apparent cross sections for electron excitation of ground-state Xe $5p^6$ to the Xe $5p^6 6p$ levels and demonstrated that the cross sections are strongly affected by the xenon target gas pressure and by the optical radiation pathway of the particular experiment. Pressure and pathway determine the optical opacity along the line-of-sight of the experiment. The observed radiation trapping effects occurred despite the fact that the emission lines investigated in their work involved near-infrared transitions to the excited Xe $5p^5 6s$ levels, and are thus only indirectly coupled to the ground state of the atom. Consequently, emission cross sections determined in one experiment do not apply to experiments run at different optical opacity conditions. Furthermore, models have not included ion-atom collision excitation [processes (6) through (8)], and no measurements are known to us that provide the respective cross sections in the energy interval of tens to hundreds of eV.

The measurement of luminescence spectra associated with processes (1)–(8) as a function of collision energy represents a first step toward determining the utility of a passive optical diagnostic method for Xe-propelled HETs. If the observed spectra exhibit significant differences for different processes, and are considerably dependent on the collision energy within a range pertinent to the thruster, analysis of the thruster's emission spectra could provide information about its microscopic parameters such as the electron energy distribution, plasma densities, and ion charge ratios. Preliminary experimental results[14] from our laboratories have demonstrated nicely that the luminescence spectra associated with ground-state target atoms [processes (1), (2), and (6)–(8)] exhibit marked differences in the near-infrared (NIR) and visible (VIS) depending on the excitation species and energy, thereby establishing the plasma diagnostic value of these measurements. Most notably, relatively high NIR emission cross sections were measured for $Xe^+ + Xe$ collisions, suggesting that ionic collisions contribute significantly to the thruster radiance, particularly in plasma regions with low electron temperatures where ion collision rates at energies above emission excitation thresholds can compete with electron excitation rates. All previous efforts in diagnosing thruster emissions only considered electron excitation functions.

In the present paper, NIR and VIS emission lines, observed in single-collision beam experiments for processes (1), (2), and (6)–(8), are evaluated with respect to their diagnostic value. Qualitative comparison is provided between spectra obtained in the beam experiments and recordings made from the discharge and plume of a TSNIIMASH D-55 anode layer thruster (TAL).[21–24] We have identified 8 NIR and 12 VIS lines associated with dissimilar upper states for which emission excitation cross sections are tabulated for a significant number of electron energies ranging from 10 to 70 eV. Additionally, for the same lines, emission excitation cross sections are provided for ion-atom collisions at a single value of the ion energy per unit charge, $E/q = 300$ eV, a typical value for HETs. This is justified given the weaker energy dependence of the respective ion collision cross sections at the high energies and the relatively narrow ion energy distribution in a nondisturbed HET.[25–27]

Because the beam experiments are conducted at substantially higher pressures in comparison with typical HET operating conditions, the pressure dependence of the measured apparent cross sections must be elucidated in detail. All tabulated values are zero-pressure extrapolated (optically thin limit). A semiempirical analytical expression is derived that renders the pressure and energy dependence of radiation trapping effects and thus permits utilization of the cross sections at experimental conditions that are not optically thin.

In a companion paper (Part II),[28] a simple CRM is proposed and implemented in the analysis of spectra observed from a D-55 TAL. The model is based on the present cross sections and a qualitative analysis of the xenon species excitation and deexcitation mechanisms in the HET plasma, including effects due to long-lived metastables.

II. EXPERIMENT

A. Luminescence experiment

The luminescence experiments at the Air Force Research Laboratory consist of propagating an electron or ion beam through a collision cell containing a Xe target gas. Figure 1 is a schematic of the collision cell providing the important dimensions to allow assessment of the radiation path lengths. The collision cell has highly reflective inner surfaces and is

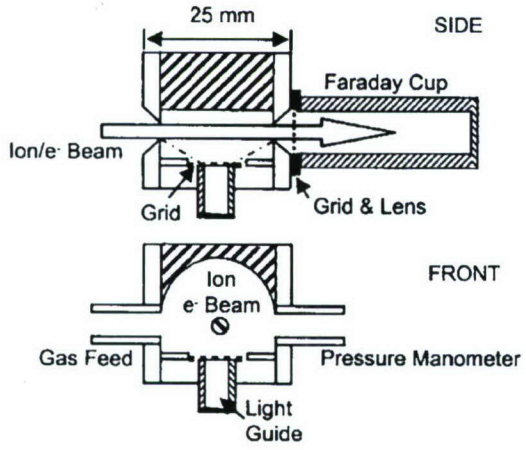

FIG. 1. Schematic representation of the target gas cell used in beam luminescence studies. Side (top) and front (bottom) views are drawn on the same scale. The plate with the exit aperture is electrically insulated from the rest of the cell to assess beam divergence.

coupled via a fused silica fiber bundle to a 0.156 m ($F/3.7$) Czerny-Turner spectrograph that is positioned outside the vacuum chamber. The spectrograph is equipped with a Princeton Instruments liquid nitrogen-cooled charge-coupled device (CCD) array detector. The emission spectrum is obtained following the subtraction of a background spectrum that is measured at the same conditions as the luminescence spectrum but with the charged particle beam deflected off the instrument axis. For the investigated spectral ranges, a 50 μm slit was used. Dependent on the wavelength range, we used a 1800 groove/mm grating with either a 400 nm or 500 nm blaze, or a 1200 groove/mm grating with a 600 nm blaze. The spectral resolution [full width at half maximum (FWHM)] is ~0.07 nm for wavelengths $\leq$800 nm and decreases to ~0.10 nm for wavelengths >800 nm.

The electron source consists of an electron gun followed by a three-element lens system that produces an electron beam of ~1 eV FWHM. In the electron beam experiments, a target cell entrance aperture of 0.165 cm diameter is used. The Xe gas pressure in the cell is measured with a capacitance manometer and did not exceed 2 mTorr, thereby ensuring single-collision conditions. The electron beam current is monitored both on a Faraday cup following the exit aperture of the collision cell, and on the cell exit aperture, which is electrically insulated from the cell. The comparison of the two currents allows quantification of the beam divergence, which is particularly important at the lowest electron energies of the present work. The electron beam energies are controlled by the dc potential difference between the electron source anode and the collision cell.

Ion-induced luminescence spectra are measured using a previously described setup at the Air Force Research Laboratory.[29,30] A xenon ion beam is generated in a dc plasma discharge ion source. The $Xe^+ + Xe$ emission cross sections are found to be independent of the source anode voltage between 25 and 85 V. The discharge is the most stable at 85 V. The ion beam is accelerated into a Wien velocity filter for ion charge state selection, then decelerated to the desired energy and propagated through the collision cell equipped with a 0.3 cm diameter aperture. Xenon target pressures similar to those in the electron beam experiments are used.

The wavelength is calibrated using emission lines from mercury and neon lamps. The spectral response of the detector is determined using a halogen-tungsten lamp. All emission spectra are normalized with respect to the exposure time, ion beam current, and the spectral response of the detector. The normalized line intensities are converted to the line excitation cross sections using the single-collision expression

$$\sigma_l = \frac{I_l F_b}{I_b N_{0b} G_b h \nu_l}, \tag{9}$$

where σ_l is the energy dependent emission cross section at the frequency ν_l, I_l is the normalized experimental emission intensity in energy units per second, I_b is the beam intensity (particles/s), N_{0b} and G_b correspond to the gas number density and an experimental geometric factor associated with the light collection efficiency, respectively, and F_b is the beam divergence factor which is dependent on the beam energy. Divergence factors of $F_b=1$ and $F_b=0.16$ are determined for 70 and 15 eV electron beams, respectively. The geometric factor G_b consisting of the product of the effective solid angle and the effective path length is determined from absolute electron-induced emission intensities observed for several transitions at 30 eV and the corresponding apparent NIR emission cross sections measured by Fons and Lin[20] extrapolated to zero pressure. In both the present experiment and that of Fons and Lin, the low-pressure limit of experimental sensitivity was 0.1 mTorr. The calibration, pressure dependence measurements, and comparison with experimental cross sections reported by Fons and Lin will be discussed in detail in Sec. III B.

B. Hall thruster experiment

Optical spectra of the D-55 TAL were recorded at the TSNIIMASH test facility. The vacuum chamber was equipped with a large window for optimal data acquisition in the TAL near-field plume and discharge regions. General features of the TALs as well as detailed information about their design and performance characteristics may be found in the literature.[21–24] The TAL spectra used for qualitative comparision with beam luminescence spectra were recorded using an Ebert-Fastie 0.5 m $F/6$ scanning monochromator that was equipped with a commercial photomultiplier tube (PMT). The monochromator had two exchangeable gratings with 1200 grooves/mm optimized for working in the VIS and IR spectral regions. The PMT had a multialkaline photocathode, providing high response from the VIS through the NIR wavelength region. Radiation from the TAL plasma was focused at the monochromator entrance slit with the use of a quartz lens, which improved the light collection efficiency and confined the instrument field of view. Entrance and exit slits of the monochromator were set between 0.05 and 0.4 mm to optimally meet the requirements of high signal-to-noise ratio and satisfactory spectral and spatial resolutions. The wavelength resolution varied from about 0.1 nm

in the TAL discharge spectra to about 1 nm in those plume spectra with the lowest radiation intensities. The discharge region covered by the monochromator aperture was about 5×5 mm, while a 20–30 mm plume scalar region was projected onto the monochromator aperture.

Ne–, Xe–, and Hg–Ar discharge lamps were used for wavelength calibration. The TAL spectrum is very dense, thus leading to important higher-order emissions from strong near UV and VIS lines. These lines were carefully filtered in the VIS and NIR regions. The spectral response of the instrument, including all optical elements and windows, was routinely measured. This was accomplished by replacing the thruster with a calibrated halogen-tungsten lamp.

Due to sputtering, the test facility window experienced loss of transparency in some long duration experiments. Variation of the window transparency in these experiments was carefully monitored. TAL discharge spectra were periodically recorded at reference operating conditions characterized by highly stable radiation intensity. Precautions were undertaken to ensure that radiation reflected from the test chamber walls did not interfere with the radiation measured from the TAL plume plasma. In order to block the reflected discharge radiation, the vacuum chamber walls were covered with highly absorbing black paint and a simple optical trap was mounted along the line of sight of the spectrometer. In addition, dedicated tests were carried out that failed to detect reflected radiation at levels exceeding 5% of the true plume signal.

A thorough investigation was conducted to determine the background pressure above which the Xe I emissions were affected by radiation trapping effects. The background pressure was changed by either varying the xenon mass flow rate or reducing the number of vacuum pumps serving the chamber while acquiring spectra. The variation of the relative intensities of the Xe II and Xe III lines was insignificant over the investigated background pressure range of $p = 0.06–0.15$ mTorr. Relative intensities of the Xe I lines remained almost constant up to a pressure of about 0.12 mTorr, above which intensities grew slightly (10%–15%) when the pressure was raised to 0.15 mTorr. It is, therefore, concluded that at pressures below 0.15 mTorr, radiation trapping effects were negligible in the TAL emission measurement. All measurements discussed in the present paper were acquired at lower background pressures.

III. RESULTS

A. Qualitative comparison of beam luminescence and TAL radiation spectra

Figure 2 compares luminescence spectra observed over the VIS and NIR spectral ranges for 300 eV $Xe^+ + Xe$ [process (6)], 600 eV $Xe^{2+} + Xe$ [processes (7) and (8)], 15 eV $e^- + Xe$, and 70 eV $e^- + Xe$ collisions [processes (1) and (2)] at near single-collision conditions. The ion collision energies are representative of typical Hall thruster operating conditions. The spectra are all corrected with respect to spectral sensitivity. It is readily seen in Fig. 2 that the four luminescence spectra are significantly dissimilar, both in relative and absolute intensities. While the ion-induced cross sections do not vary greatly with energy at the respective high energies, this is not the case for the relevant electron energies, as the marked difference between the 15 and 70 eV spectra demonstrates. The 15 eV e^- and 300 eV Xe^+-induced spectra are the simplest where significant intensities are only observed above ~800 nm when the spectra are plotted on a linear intensity scale, as in Fig. 2. The high relative intensity of the NIR lines is not surprising since they are associated with transitions from the lowest excited $5p^5 6p(6p')$ levels that have excitation energies between 9.6 and 11.2 eV. The electron collision spectrum obtained with 70 eV electrons exhibits a dense VIS spectrum, but the NIR emissions are still the most intense. Many of the VIS lines are produced in process (2) and associated with Xe II ionic emissions. In case of the $Xe^{2+} + Xe$-induced emissions, the VIS spectrum also contains important Xe II contributions. The significant Xe II emission intensities suggest that process (8) might play a role in HETs along with the primary Xe II excitation mechanism (3). Process (8) is exothermic by ~9 eV, and, therefore, excitation of one of the product Xe^+ ions can occur with little energy transfer. The asymmetric charge exchange cross section at $E/q = 300$ eV was determined to be 2.8 ± 0.9 Å.[2,31]

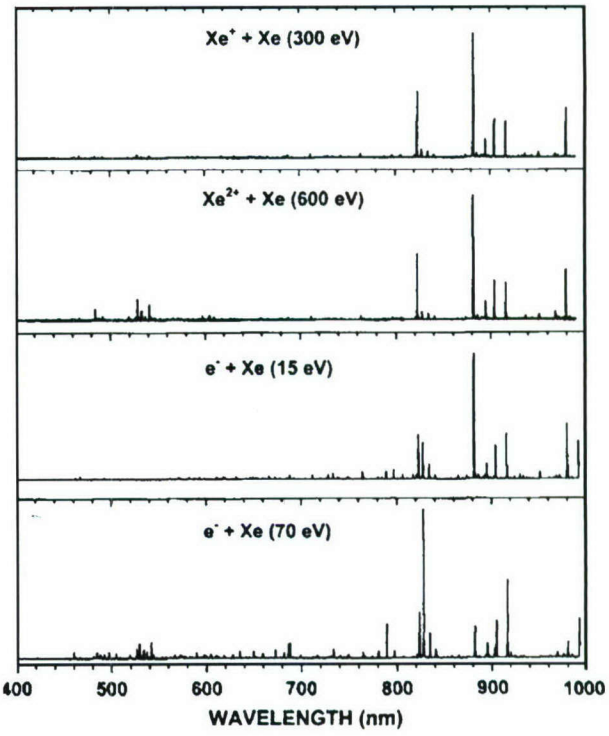

FIG. 2. Comparison of Xe beam luminescence spectra at representative energies covering the full spectral range of the present study. The intensities are plotted on a relative, linear scale.

Figure 3 compares beam measurements to typical spectra observed in the discharge and plume of the TAL in the NIR spectral region. The beam experiment spectra are normalized with respect to the ion beam current and target gas pressure of each respective measurement and are plotted on an absolute intensity scale. The line near 970 nm and some other lines in the longer wavelength region of the $Xe^{2+} + Xe$ spectrum are attributable to second order emissions of corre-

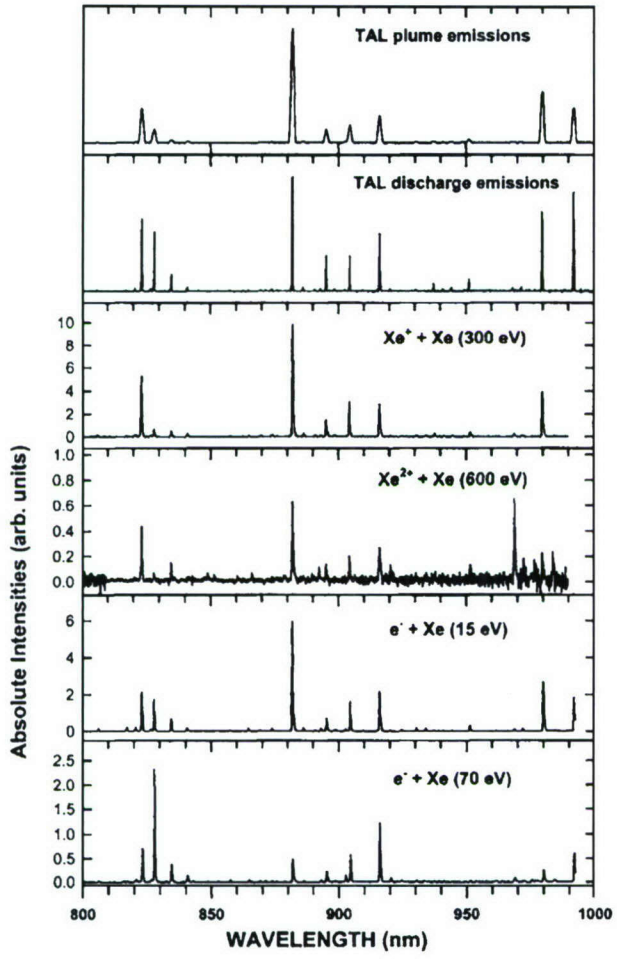

FIG. 3. Comparison of TAL discharge and plume spectra with Xe beam luminescence spectra at representative energies in the 800–990 nm spectral range (NIR). The beam spectra are plotted on the same absolute intensity scale (normalized with respect to neutral density and beam intensity).

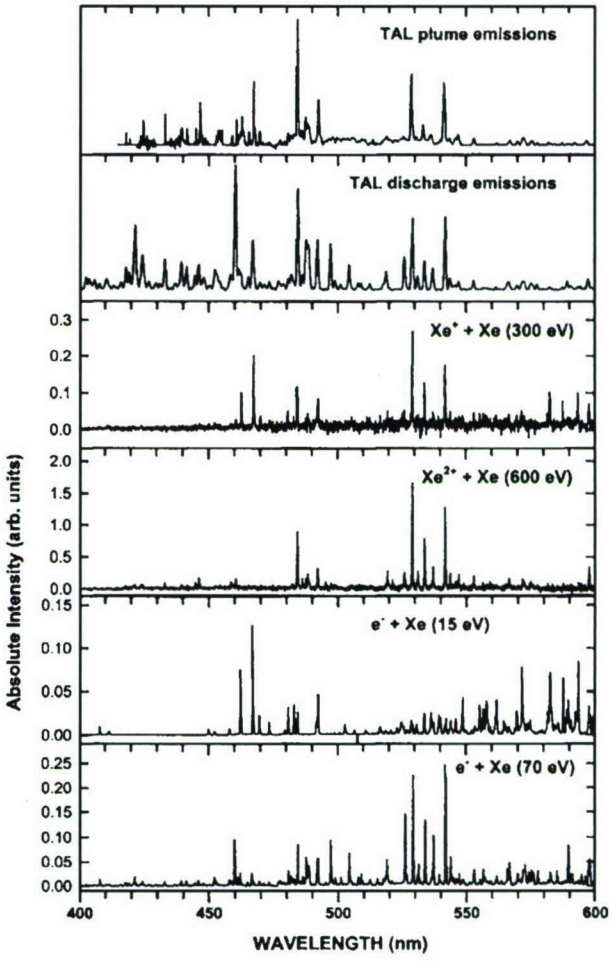

FIG. 4. Comparison of TAL discharge and plume spectra with Xe beam luminescence spectra at representative energies in the 400–600 nm spectral range (VIS). The beam spectra are plotted on the same absolute intensity scale (normalized with respect to neutral density and beam intensity).

sponding strong lines in the VIS region of the spectrum. It is seen that the absolute intensities of the Xe^+-induced emissions are comparable with the 15 eV electron impact excitation intensities, a first hint that 300 eV Xe^+ may produce excitation rates that are competitive with those of electrons at low electron temperatures.

All four luminescence spectra exhibit marked differences in the relative intensities of the NIR lines. The relative intensities of the discharge spectrum of the thruster compare qualitatively closest to the e^- (15 eV) spectrum. Meanwhile, the plume NIR spectrum appears to be composed of a combination of Xe^+ and low-energy ($\sim$15 eV) electron-induced emissions, as best observed by comparing the intensities of the lines at 823 and 828 nm. The ratio I_{823}/I_{828} increases rapidly when the electron energy is decreased from 70 to 15 eV. At 15 eV, however, the ratio is still smaller than that observed in the TAL plume spectrum in Fig. 3. The Xe^+-induced spectrum exhibits the highest I_{823}/I_{828} ratio, and thus a combination of the 15 eV electron and the ion-induced spectrum is capable of reproducing the TAL plume ratio. Thus, already a qualitative analysis of the spectra in Fig. 3 suggests that ion-atom collisions are an important contributor to HET plasma emissions.

Figure 4 compares TAL discharge and plume spectra to beam luminescence spectra in the 400–600 nm range. In this wavelength region, the TAL discharge emission spectrum resembles more closely the 70 eV electron-induced spectrum. The VIS plume spectrum, on the other hand, exhibits many features observed in the $Xe^{2+}+Xe$ luminescence spectrum. This is not surprising, because the VIS spectrum is featured by strong Xe II emissions. However, caution is advised in drawing conclusions from the resemblance between beam and TAL spectra in regions of the spectrum where Xe II are present because the excitation of xenon ions by electron impact [process (3)] is likely to play a more important role given the high ionization fraction in HET plasmas and the lower excitation energies associated with electron-ion luminescent collisions. This is further discussed in Part II.[28]

B. NIR emission cross sections

As demonstrated in Fig. 3, the NIR Xe I emission line intensities have promising plasma diagnostic properties. Meanwhile, the NIR spectrum is not congested so that a spectrometer with modest resolution can record accurate intensities. The most intense lines are associated with emis-

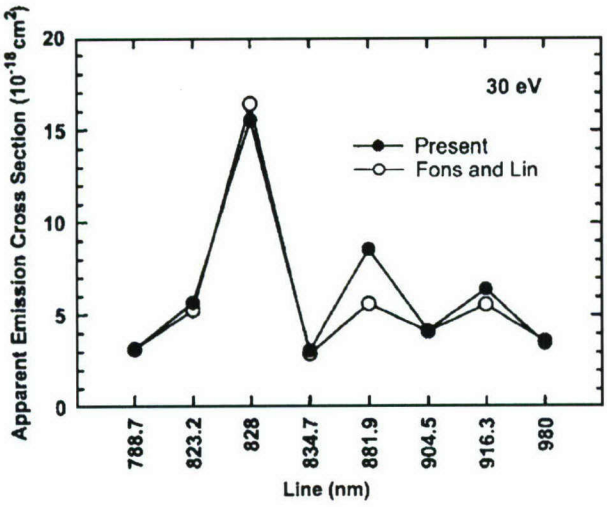

FIG. 5. Comparison between present scaled electron impact apparent emission excitation cross sections of the respective NIR lines at 30 eV to those derived from the measurements of Fons and Lin (see Ref. 20).

sions from the $2p_i$ (Paschen notation) excited states, for which Fons and Lin conducted an extensive study on the electron excitation cross sections.[20] Those measurements are used to calibrate the geometric factor G of the present experiment [Eq. (9)]. An important problem affecting the derivation of useful cross sections for these lines is the significant pressure dependence at the conditions of beam experiments. As demonstrated by Fons and Lin,[20] the pressure dependence is associated with radiation trapping effects due to cascade transitions from states that are optically coupled to the ground state. Fons and Lin[20] examined the radiation trapping effects of all lines associated with the $2p_i$ levels at electron energies of 30 and 50 eV. The G factor of the present experiment is calibrated by recording measurements for pressures ranging from 0.1 to 2 mTorr at an electron energy of 30 eV and scaling the measurements extrapolated to zero pressure to the same NIR line excitation cross sections reported by Fons and Lin. This leads to an agreement within 10% for all lines except the $2p_8$ emissions at 881.9 nm, where the present measurements lead to ~50% higher cross sections. We do not have an explanation for this discrepancy. The comparison between the present, scaled emission excitation cross sections and the zero-pressure extrapolated values of Fons and Lin is shown in Fig. 5.

For the sake of deriving reliable zero-pressure extrapolated cross sections over a large impact energy range, and for the inclusion of optical opacity effects in a CRM suited for test chamber analysis, a semiempirical model is derived with parameters that are adjusted to fit the pressure dependences recorded at electron energies of 30 and 50 eV in both the experiments of Fons and Lin, and the present experiment. The total cross section, $\sigma_t(E,p)$, excited by an electron of energy E in a Xe gas at pressure p is given by

$$\sigma_t(E,p) = \sigma_d(E) + \sigma_c(E,p), \tag{10}$$

where $\sigma_d(E)$ is the direct excitation cross section, and $\sigma_c(E,p)$ is the excitation cross section through cascade transitions from higher excited states. The latter can be written as

$$\sigma_c(E,p) = \sigma_c(E,0) + \sigma_c(E,0)f(p), \tag{11}$$

where $\sigma_c(E,0)$ signifies the pressure independent cascades that occur instantaneously after excitation, and the second term in Eq. (11) represents the cascades that occur due to reabsorption of radiation. Note that the factor $f(p)$ does not depend on energy. Equations (10) and (11) can be rewritten to

$$\sigma_t(E,p) = \sigma_t(E,0)\left[1 + \frac{\sigma_c(E,0)}{\sigma_t(E,0)}f(p)\right], \tag{12}$$

where $\sigma_t(E,0) = \sigma_d(E) + \sigma_c(E,0)$. The ratio between the zero-pressure cascade and total cross section is modeled by

$$\frac{\sigma_c(E,0)}{\sigma_t(E,0)} = A\left(\frac{E-11.5}{E-9.8}\right)^n, \quad E > 11.5 \text{ eV},$$
$$\frac{\sigma_c(E,0)}{\sigma_t(E,0)} = 0, \quad E \leqslant 11.5 \text{ eV}, \tag{13}$$

where 9.8 and 11.5 eV represent the average excitation energies of $2p_i$ and cascade levels, respectively. $f(p)$ is proposed to be represented by

$$f(p) = C(1 - e^{-\gamma p})^2. \tag{14}$$

Equation (13) captures the threshold behavior of emission cross sections while Eq. (14) simulates the growth in pressure effect that eventually terminates at a value C. n and γ are curvature parameters. The $(1-e^{-\gamma p})$ factor describes the radiation trapped in the viewing volume in a single emission-reabsorption cycle. The exponent associated with the factor describes the average number of such cycles. Since it is found that setting the exponent equal to 1 or 2 does not make a significant difference in the quality of the fits, the exponent was set to 2 to minimize the number of adjustable variables. The final semiempirical expression for $E > 11.5$ eV is then given by

$$\sigma_t(E,p) = \sigma_t(E,0)\left\{1 + a\left(\frac{E-11.5}{E-9.8}\right)^n (1 - e^{-\gamma p})^2\right\}, \tag{15}$$

where $a = AC$. The adjustable parameters that are independent of energy are determined in an iterative procedure to reproduce the pressure dependences at 30 and 50 eV for the two experimental sets. Note that γ depends on the effective pressure, which is the pressure integrated along the radiation transmission path. Consequently, it depends on the experimental geometry.

Figure 6 is an example of a fit of Eq. (15) to present measurements of the pressure dependence of the apparent excitation cross section of the $2p_9$ level, as measured on the 904.5 nm line at an electron impact energy of 50 eV. The apparent excitation cross section of this level exhibits a strong pressure dependence. The present cross sections are significantly lower than the values determined by Fons and Lin,[20] suggesting higher optical opacity in their experiments given the relatively good agreement at 30 eV.

Having determined the constants a, n, and γ, the zero-pressure cross sections corresponding to the optically thin limit can be determined from the electron energy dependence

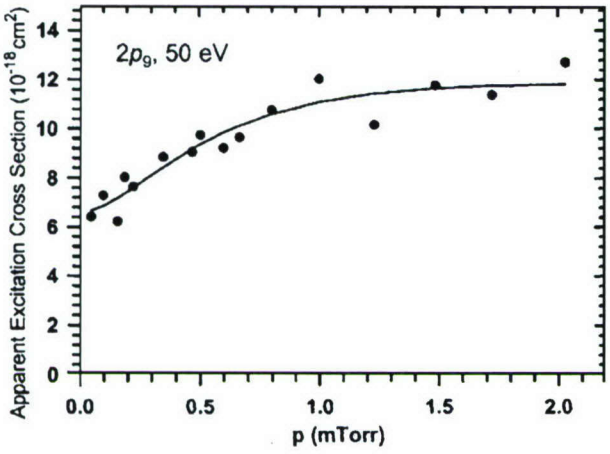

FIG. 6. Pressure dependence of the $2p_9$ level apparent emission excitation cross section for 50 eV electrons (filled circles). The solid line is the modeled pressure dependence using Eq. (15).

of apparent emission cross sections measured at target gas pressures at which adequate signal levels are achieved. The zero-pressure cross sections derived from present measurements at 1.45 mTorr are shown in Table I for eight selected lines with appreciable intensities. The lines have been chosen to be from different upper states of the $2p_i$ series, thus ensuring that each line is associated with a different excitation history. The upper states are also listed in the table along with the respective excitation energies. The calibration of the spectral sensitivity was validated by measuring branching fractions for lines stemming from the same excited state. Good agreement exists with branching fractions measured by Fons and Lin and others reported in the literature.[32] The table also lists the adjustable parameters in Eq. (15) that describe the pressure dependence. In all cases, Eq. (15) is found to produce a satisfactory representation of the measured pressure dependence.

Having calibrated the collection efficiency of the present optical experiment based on the cross section measurements by Fons and Lin,[20] first measurements of ion-induced emission cross sections were possible. Table I also lists the apparent emission excitation cross sections for 300 eV (E/q) ions. The pressure dependence of the respective cross sections was also examined. No significant cross-section growth with pressure could be identified at the same cell pressures examined in the electron beam work. A cursory look at the energy dependence of the emission cross sections was also conducted. The ion-induced emissions gradually increase between 100 and 300 eV; however, the increase is such that,

TABLE I. Emission cross sections in units of 10^{-18} cm^2 for selected $5p^56p(p')$ (Paschen notation: $2p_i$) NIR lines at selected electron energies, $E(e^-)$, and for E/q=300 eV xenon ions. All cross sections correspond to zero-pressure values. The original spectra were recorded at a cell pressure of 1.45 mTorr and converted to zero-pressure values using parameters a, n, and γ of Eq. 15, for energy in units of eV, cross section in 10^{-18} cm^2, and pressure in mTorr. E_0 is the excitation energy of the respective level.

		Lines							
	λ (nm)	788.7	823.2	828.0	834.7	881.9	904.5	916.3	980.0
$E(e')$	Upper level	$2p_1$	$2p_6$	$2p_5$	$2p_3$	$2p_8$	$2p_9$	$2p_7$	$2p_{10}$
(eV)	E_0 (eV)	9.57	9.82	9.93	11.05	9.72	9.69	9.79	9.58
10		0.002	0.037	0.23	0.010	0.093	0.024	0.038	0.047
12		0.006	2.23	1.68	0.02	7.01	1.28	1.54	2.29
15		1.09	11.35	9.42	3.96	37.40	7.14	12.95	18.09
17		1.49	13.14	12.01	4.83	38.80	8.78	15.09	17.05
19		1.79	12.89	14.89	5.08	34.30	8.87	14.91	14.17
21		2.39	11.63	17.94	5.05	26.90	8.18	13.61	11.19
23		2.92	9.58	18.47	4.49	19.92	7.11	11.02	7.98
25		3.54	7.84	18.77	4.03	15.29	6.22	9.27	6.06
27		3.19	6.03	16.80	3.14	10.21	4.74	7.06	4.13
29		3.21	5.76	16.01	3.07	8.99	4.28	6.58	3.58
31		3.05	5.55	15.05	3.04	8.13	4.04	6.24	3.32
35		2.71	5.15	13.39	2.94	6.54	3.66	5.52	2.48
40		2.05	4.31	11.12	2.63	4.74	2.97	4.61	2.04
45		1.78	4.11	10.42	2.45	4.33	2.57	4.37	1.87
50		1.70	3.81	9.74	2.29	3.97	2.23	4.10	1.74
55		1.77	3.74	9.72	2.26	3.90	2.10	3.98	1.75
60		1.98	3.52	9.26	2.12	3.59	1.90	3.66	1.56
65		1.67	2.96	7.92	1.81	2.86	1.56	3.17	1.34
70		1.16	2.62	7.18	1.60	2.41	1.34	2.82	1.14
	a	1.394	1.356	1.297	0.275	0.768	3.669	3.000	1.354
	n	19	15	16	8	13	35	15	8
	γ	0.75	0.65	1.47	2.00	0.69	2.56	2.02	1.70
Ion Excitation									
Xe^+		0.942	29.23	3.90	3.13	69.11	18.67	20.73	32.71
Xe^{2+}		0.244	10.1	1.00	1.02	18.31	5.70	9.31	6.75

TABLE II. Emission cross sections in units of 10^{-18} cm^2 for selected VIS lines at selected electron energies, $E(e^-)$, and for $E/q=300$ eV xenon ions. The spectra were recorded at a cell pressure of 1.5 mTorr. E_0 is the excitation energy of the respective level from the ground state of the atom or ion. All energy values are in eV.

		Xe(I) lines				Xe(II) lines							
	λ (nm)					484.4	492.1	497.3	504.5	519.1	526.2	529.2	541.9
	Upper level	462.4 $3p_6$	467.1 $3p_8$	473.4 $2p_3$	480.7 $3p_5$	$6p$ ($^4D^0_{7/2}$)	$6p$ ($^2D^0_{5/2}$)	$6p'$ ($^2P^0_{3/2}$)	$6p'$ ($^2P^0_{1/2}$)	$6p$ ($^4D^0_{1/2}$)	$6p'$ ($^2D^0_{3/2}$)	$6p$ ($^4P^0_{5/2}$)	$6p$ ($^4D^0_{5/2}$)
$E(e^-)$	E_0	10.99	10.97	11.05	11.01	14.10	15.26	16.08	16.46	14.93	16.36	13.89	14.07
10		0.000 16	0.000 46	0.000 17	0.000 13	0.001 42	0.000 54	0.000 24	0.000 21	0.000 13	0.000 69	0.005 28	0.003 71
15		0.43	0.75	0.09	0.17	0.17	0.28	0.005	0.003 7	0.01	0.10	0.07	0.19
20		0.45	0.51	0.11	0.19	0.18	0.29	0.005	0.004 0	0.01	0.09	0.08	0.18
25		0.38	0.34	0.11	0.27	0.18	0.24	0.003	0.002 3	0.01	0.06	0.14	0.17
27		0.36	0.29	0.10	0.29	0.39	0.31	0.02	0.01	0.07	0.13	0.88	0.93
30		0.30	0.30	0.10	0.27	0.69	0.59	0.20	0.11	0.28	0.63	1.89	1.93
35		0.23	0.36	0.11	0.23	0.91	0.80	0.52	0.31	0.51	1.16	2.56	2.76
40		0.21	0.49	0.10	0.21	0.96	0.94	0.93	0.61	0.68	1.68	2.87	3.09
45		0.21	0.55	0.10	0.20	0.82	0.88	1.09	0.77	0.68	1.71	2.55	2.77
50		0.21	0.51	0.09	0.20	0.68	0.77	1.03	0.72	0.60	1.54	2.15	2.48
55		0.21	0.45	0.09	0.19	0.59	0.68	0.92	0.65	0.53	1.37	1.89	2.26
60		0.20	0.40	0.08	0.18	0.52	0.61	0.83	0.57	0.49	1.25	1.71	2.10
65		0.16	0.33	0.07	0.15	0.42	0.51	0.68	0.47	0.42	1.04	1.40	1.80
70		0.15	0.31	0.06	0.14	0.39	0.47	0.65	0.45	0.41	0.98	1.29	1.69
Ion Excitation													
Xe^+		0.63	1.31	0.19	0.28	0.83	0.58	0.10	0.03	0.29	0.22	1.34	1.02
Xe^{2+}		1.48	2.45	0.23	0.03	21.8	9.4	3.17	1.82	8.83	8.28	40.3	33.6

when convoluted with a typically observed ion energy distribution[25–27] of a Hall thruster operated at 300 V, the application of the present values at 300 eV per charge unit is sufficiently accurate for modeling purposes.

Table II lists the emission cross sections determined for specific VIS lines with potential diagnostic value. Cross sections could only be determined for lines at wavelengths where the spectral sensitivity could reliably be determined with our halogen tungsten lamp ($\lambda > 450$ nm). VIS lines associated with the same upper state of a NIR line with known branching ratios were also used to ensure that the VIS spectral sensitivity was properly defined. The selected emission lines at 462.4, 467.1, 473.4, and 480.7 nm are associated with neutral excited states with excitation energies between 10.97 and 11.05 eV. The emission lines at 484.4, 492.1, 497.3, 504.5, 519.1, 526.2, 529.2, and 541.9 nm stem from $6p$ ionic states, respectively, with excitation energies ranging from 13.89 to 16.46 eV. These excitation energies correspond to electron impact ionization thresholds between 25.02 and 28.59 eV in reaction (2). For some ionic lines, the cross sections do not drop to zero at electron energies significantly below the nominal threshold. This can be attributed to interfering neutral lines. For example, a $6s-7p$ neutral line at 484.3 nm is responsible for prethreshold signal recorded for the 484.4 nm ionic line. A higher resolution experiment would be required to deconvolute the two contributions. Equally, the 526.2, 529.2, and 541.9 nm ionic lines are subject to contributions from weak neutral emissions at 525.1, 527.3, 528.6, 541.8, and 542.2 nm, respectively.

The pressure dependence was also examined for a number of lines listed in Table II. The variation of emission cross section with pressure in the 0.1–2 mTorr range of the beam experiment was negligible in all listed cases except for minor pressure effects for the $2p_3$ line at 473.4 nm. A CRM for the VIS region of the spectrum, therefore, can apply the cross sections of Table II without pressure correction.

IV. DISCUSSION

We present electron and ion-beam-induced luminescence spectra in a xenon gas at single-collision conditions at controlled beam energies. VIS and NIR spectra exhibit a marked dependence on excitation energy and species, suggesting that the spectra provide information on plasma parameters such as electron temperature and charge state densities. The spectra were used to derive emission cross sections for a set of VIS and NIR lines. Use of the emission cross sections in a CRM must take pressure dependences of the apparent emission cross sections into effect, since the magnitude of radiation trapping effects is highly line dependent. The electron emission excitation cross sections for the NIR lines confirm important radiation trapping effects recently reported by Fons and Lin.[20] These authors attribute the radiation trapping effects to cascade transitions from higher lying states that populate the $5p^5 6p(6p')$ levels that are the upper states of the prominent NIR lines. The upper states of some cascade transitions are optically coupled to the ground state through vacuum ultraviolet transitions. Because the radiation due to transitions to the ground state can be reabsorbed by ground-state xenon atoms, successive absorption of the emitted vacuum ultraviolet photons increases the effective branching ratio in favor of cascade transitions, thereby increasing the

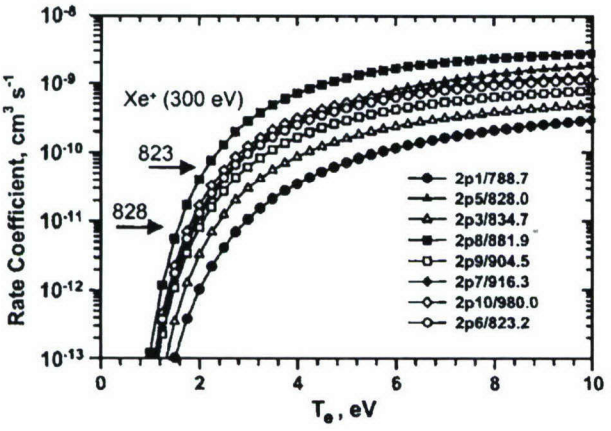

FIG. 7. Electron temperature dependence of Xe NIR line excitation rate coefficients in the optically thin limit. The lines are identified with Paschen notation ($2p_i$) of the upper level and the respective wavelength in nm. The horizontal arrows indicate excitation rate coefficients for 300 eV Xe^+ impact for the 823.3 and 828.0 nm lines (see Table III).

probability of emission in the NIR lines. The pressure dependence is weakest for the 881.9 nm emission line that is associated with the $2p_8$ $J=3$ level that is coupled to the ground state via a minimum of three transitions while all other levels ($J<3$) have possible two-step (excitation, followed by cascade transition to $2p$ level) mechanisms.

The present electron-induced emission cross sections were calibrated by comparison with the results presented by Fons and Lin at 30 eV extrapolated to zero pressure.[20] This provided a good agreement for all line excitation cross sections except for the the $2p_8$ emissions at 881.9 nm, where the present measurements are ~50% higher at low electron energies. The present higher values are supported by the fact that the model developed in Part II either slightly underestimates or agrees with the 881.9 nm intensity observed in TAL plumes and discharges, respectively. Probably the most significant findings of the present paper are the high NIR emission cross sections for Xe^+ ions. For all of the selected eight NIR lines, no radiation trapping effects were detected at the high ion energy of 300 eV per charge unit. The lack of pressure effects on the apparent cross sections is not surprising given the different mechanisms associated with electron and ion-atom inelastic scattering. In the case of electrons, the direct interaction between the incident electron and the atomic electrons is responsible for the electronic excitation in the atom. At the present ion energies, the ion velocity is significantly lower than the velocities of the electrons that are excited in the atom. In this low-velocity limit of ion-atom collisions, inelastic scattering is induced by nonadiabatic interactions that increase with the relative nuclear velocity.[33,34] Consequently, the excitation cross sections increase with ion energy and peak at energies much higher than observed for electron collisions. In the present experiment, the ion emission excitation cross sections increase in the ion energy (E/q) range from 100 to 300 eV. Thus, cascade contributions can be assumed to be much weaker for the ion emission excitation cross sections.

The significance of the high ion emission cross sections can be demonstrated by comparing the excitation rate coefficients for electron and ion impact. Assuming a Maxwellian electron energy distribution and single ion energy, they are given by

$$k_e = \int_0^\infty 2E \sqrt{\frac{2}{\pi (kT_e)^3 m_e}} \exp\left(-\frac{E}{kT_e}\right) \sigma_e(E) dE, \tag{16}$$

$$k_{\text{ion}} \approx \sigma_{\text{ion}}(eV) \sqrt{\frac{2qeV}{M}}, \tag{17}$$

where T_e is the electron temperature, k is the Boltzmann constant, V is the acceleration voltage, M is the mass of the xenon ion, and m_e is the rest mass of the electron. The electron temperature dependences of the rate coefficients calculated for electron impact NIR line excitation using the present cross sections for optically thin conditions are shown in Fig. 7. Note that the logarithmic scale obscures the important relative line excitation rate dependencies which are discussed extensively in Part II. The rate coefficients for ion impact excitation are listed in Table III. From the comparison between the electron and Xe^+ impact excitation rate coefficients, it is seen that they are equal for the different NIR lines at temperatures ranging between 1.9 and 2.7 eV. The horizontal arrows in Fig. 7 point out the 300 eV Xe^+ impact rate coefficients for the 828.0 and 823.2 nm lines. Thus, a passive optical analysis of a Xe plasma characterized by low electron temperatures (<10 eV) using the present intense NIR lines has to include the ionic contributions. This is further discussed in Part II. Meanwhile, metastable population, in particular population of the $1s_5$ state, which is the lower state of the 823.3, 881.9, 904.5, and 980.0 nm transitions, have important effects on the relative intensities of the lines in the plasma. A quantitative analysis is also provided in Part II.

As the cross sections listed in Table II demonstrate, VIS emission excitation rates associated with ground-state xenon atoms are significantly lower. The largest cross sections are found for Xe^{2+} excitation of ionic lines, mostly likely attributable to the asymmetric charge exchange process [Eq. (8)].

TABLE III. NIR ion impact emission excitation rate coefficients for $E/q=300$ eV xenon ions. Rate coefficients are given in units of 10^{-11} cm^3 s^{-1}.

	Lines							
λ (nm)	788.7	823.2	828.0	834.7	881.9	904.5	916.3	980.0
Upper level	$2p_1$	$2p_6$	$2p_5$	$2p_3$	$2p_8$	$2p_9$	$2p_7$	$2p_{10}$
Xe^+	0.198	6.14	0.819	0.656	14.5	3.92	4.35	6.87
Xe^{2+}	0.072	3.01	0.296	0.304	5.44	1.69	2.76	2.00

The markedly different spectra induced by the singly and doubly charged ion suggest that an analysis of the VIS spectrum in the plume of the Hall thruster may provide information on the ionic charge state distribution. For example, the XeI line at 467.1 nm is prominent in the Xe^+ luminescence spectrum, while the XeII line at 484.4 nm is prominent in the Xe^{2+} spectrum. An analysis based on ionic lines, however, must include electron-ion excitation processes [Eq. (3)], for which accurate cross sections are not available. Thus, until such cross sections are available, the present ion emission excitation cross sections associated with XeII lines are limited to quantitative analysis in the extreme far field of the plume where electron temperatures are very low. In the discharge, on the other hand, electron-ion collisions can be expected to dominate excitation of the XeII lines listed in Table II. In this case, XeII line emission intensities are proportional to the product of the ion and electron density, and, therefore, provide a measure of the plasma density. This is further discussed in Part II.

V. CONCLUSIONS

We report a comprehensive set of XeI/XeII emission excitation cross sections for electron and ion impacts with ground-state Xe atoms. The electron-impact luminescence spectra are found to depend significantly on electron energy. Ion-induced spectra at the typical Hall thruster acceleration energy of $E/q=300$ eV are also markedly different from the electron excitation spectra. We distinguish between the VIS and NIR spectral regions. The electron energy dependence from threshold to 70 eV is reported for 12 VIS lines and 8 NIR lines. The lines are chosen with respect to their prominence in the spectrum and the uniqueness of the upper levels. The NIR electron emission excitation cross sections exhibit a significant pressure dependence in the cell pressure range of 0.1–2 mTorr, confirming the observations by Fons and Lin.[20] The pressure dependence is attributed to radiation trapping involving cascade transitions from levels that are optically coupled with the ground state. A simple empirical expression is derived that accounts for the energy dependence of radiation trapping effects. VIS line and all ion-impact excitation cross sections are not found to exhibit pressure effects at the pressures of the present experiments.

The magnitude of ion impact excitation cross sections in the NIR spectral range of the spectrum is sufficient that they must be included in a Hall thruster radiative model at low electron temperatures. To date no xenon collisional radiative models have included ion collisional excitation. The present VIS spectra suggest that ion collisions may also play an important role in this spectral range at low electron temperatures. However, since XeII lines are prominent in this spectral range, a quantitative model requires electron-Xe^+ emission excitation cross sections, which involve the lowest excitation energies for ground-state species, and therefore are expected to have the highest excitation cross sections at a particular electron energy. Such cross sections are not available in the literature, and a model including them would depend on order-of-magnitude estimates based on approximate methods.

ACKNOWLEDGMENTS

The authors thank J. Sommerville for valuable comments and suggested corrections regarding this manuscript. This work was partially funded by AFOSR under task 2303EP02 (M. R. Berman). One of the authors (G.F.K.) was supported by AFOSR through ISTC/EOARD/TSNIIMASH Partner Project 2234p (EOARD Dr. I. Wysong).

[1] A. I. Bugrova, V. A. Ermolenko, V. A. Niskin, and A. S. Sokolov, Teplofiz. Vys. Temp. **19**, 428 (1981).
[2] D. J. Manzella, *23rd International Electric Propulsion Conference, Columbus, OH, 1993*, Report No. IEPC-93-097, 1993.
[3] G. F. Karabadzhak, A. V. Semenkin, A. O. Tverdokhlebov, and D. J. Manzella, Proceedings of the 25th International Electric Propulsion Conference, Cleveland, OH, 1997.
[4] P. Leray, J. Bonnet, D. Pigache, T. Minea, J. Bretagne, and M. Touzeau, *25th International Electric Propulsion Conference, Cleveland, OH, 1997*, Report No. IEPC 97-054, 1997.
[5] N. B. Meezan, J. W. A. Hargus, and M. A. Capelli, *34th Joint Propulsion Conference, Cleveland, OH, 1998*, Report No. AIAA-98-35, 1998.
[6] F. Darnon, M. Lyszyk, and A. Bouchoule, *33rd Joint Propulsion Conference, Seattle, WA, 1997*, Report No. AIAA-97-3051, 1997.
[7] K. Komurasaki, Y. Sakurai, and D. Kusamoto, *34th Joint Propulsion Conference, Cleveland, OH, 1998*, Report No. AIAA-98-3638, 1998.
[8] N. B. Meezan, J. W. A. Hargus, D. P. Schmidt, and M. A. Cappelli, *35th AIAA/ASME/SAE/ASEE Joint Propulsion Conference, Los Angeles, CA, 1999*, Report No. AIAA-99-2284, 1999.
[9] M. Prioul, S. Roche, D. Pagnon, L. Magne, M. Touzeau, A. Bouchoule, and P. Lasgorceix, *37th AIAA/ASME/SAE/ASEE Joint Propulsion Conference and Exhibit, Salt Lake City, UT, 2001*, Report No. AIAA-2001-3358, 2001.
[10] G. F. Karabadzhak, A. V. Semenkin, and A. O. Tverdokhlebov, Third European International Propulsion Conference, Cannes, France, 2000.
[11] G. F. Karabadzhak, A. V. Semenkin, and A. O. Tverdokhlebov, *37th AIAA/ASME/SAE/ASEE Joint Propulsion Conference and Exhibit, Salt Lake City, UT, 2001*, Report No. AIAA-2001-3889, 2001.
[12] D. Pagnon, P. Lasgorceix, and M. Touzeau, *40th AIAA/ASME/SAE/ASEE Joint Propulsion Conference, Fort Lauderdale, FL, 2004*, Report No. AIAA-2004-3773, 2004.
[13] N. B. Meezan, J. W. A. Hargus, D. P. Schmidt, and M. A. Cappelli, *35th AIAA/ASME/SAE/ASEE Joint Propulsion Conference, Los Angeles, CA, 1999*, Report No. AIAA-99-2284, 1999.
[14] G. F. Karabadzhak, Y. Chiu, S. Williams, and R. A. Dressler, *37th AIAA/ASME/SAE/ASEE Joint Propulsion Conference and Exhibit, Salt Lake City, UT, 2001*, Report No. AIAA-2001-3893, 2001.
[15] A. I. Bugrova, L. M. Volkova, V. A. Ermolenko, E. A. Kralkina, A. M. Deviatov, and B. K. Khartchenkov, Teplofiz. Vys. Temp. **19**, 1149 (1981).
[16] A. I. Bugrova, V. A. Ermolenko, and A. S. Sokolov, Teplofiz. Vys. Temp. **25**, 1080 (1987).
[17] M. Gryzinski, Phys. Rev. **138**, 305 (1965).
[18] E. Bauer and C. D. Bartky, J. Chem. Phys. **46**, 2466 (1965).
[19] G. Colonna, L. D. Pietanza, and M. Capitelli, *31st AIAA Plasmadynamics and Lasers Conference, Denver, CO, 2000*, Report No. AIAA-2000-2349, 2000.
[20] J. T. Fons and C. C. Lin, Phys. Rev. A **58**, 4603 (1998).
[21] C. E. Garner, J. R. Brophy, and J. E. Pollack, *30th AIAA/ASME/SAE/ASEE Joint Propulsion Conference, Indianapolis, IN, 1994*, Report No. AIAA-94-3010, 1994.
[22] C. E. Garner, S. O. Tverdokhlebov, A. V. Semenkin, and V. I. Garkusha, *32nd AIAA/ASME/SAE/ASEE Joint Propulsion Conference, Lake Buena Vista, FL, 1996*, Report No. AIAA-96-2967, 1996.
[23] D. J. Manzella, S. Oleson, J. Sankovic, T. Haag, A. Semenkin, and V. Kim, *32nd AIAA/ASME/SAE/ASEE Joint Propulsion Conference, Lake Buena Vista, FL, 1996*, Report No. AIAA-96-2736, 1996.
[24] M. T. Domonkos, A. D. Gallimore, C. M. Marrese, and J. M. Haas, J. Propul. Power **16**, 91 (2000).
[25] I. D. Boyd and R. A. Dressler, J. Appl. Phys. **92**, 1764 (2002).
[26] L. B. King and A. D. Gallimore, J. Propul. Power **16**, 916 (2000).
[27] J. E. Pollard and E. J. Beiting, Third International Conference on Spacecraft Propulsion, Cannes, France, 2000.
[28] G. F. Karabadzhak, Y. Chiu, and R. A. Dressler, J. Appl. Phys. **99**, 113305 (2006).

[29]R. A. Dressler, J. A. Gardner, R. H. Salter, and E. Murad, J. Chem. Phys. **96**, 1062 (1992).
[30]R. A. Dressler and E. Murad, in *Unimolecular and Bimolecular Ion-Molecule Reaction Dynamics*, edited by C. T. Ng, T. Baer, and I. Powis (Wiley, New York, 1994).
[31]J. S. Miller, S. H. Pullins, D. J. Levandier, Y. Chiu, and R. Dressler, J. Appl. Phys. **91**, 984 (2002).
[32]A. A. Radzig and B. M. Smirnov, *Reference Data on Atoms, Molecules, and Ions* (Springer-Verlag, Berlin, 1985).
[33]J. B. Delos, Rev. Mod. Phys. **53**, 287 (1981).
[34]B. H. Brandsen and M. R. C. McDowell, *Charge Exchange and the Theory of Ion-Atom Collisions* (Oxford University Press, Oxford, 1992).